Sensors & Actuators: B. Chemical 431 (2025) 137428

Contents lists available at ScienceDirect

Sensors and Actuators: B. Chemical

journal homepage: www.elsevier.com/locate/snb

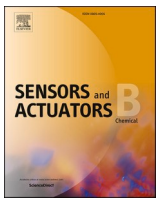

# Zeolite 5 A mediated palmitic acid detection in tomato seed oil by photoionization detector

G. Oliva [a], L. Manin [a,b], S. Valić [c], S.K. Islam [d], A.S. Fiorillo [a], S.A. Pullano [a,d,*]

[a] Department of Health Sciences, "Magna Græcia" University of Catanzaro, Catanzaro, Italy
[b] Dept. of Medical Chemistry Biochemistry and Clinical Chemistry, University of Rijeka, Rijeka, Croatia
[c] Division of Physical Chemistry, Ruđer Bošković Institute, Zagreb, Croatia
[d] Dept. of Electrical Engineering and Computer Science, University of Missouri, Columbia, MO, USA

ARTICLE INFO

*Keywords:*
Palmitic acid
Photoionization technique
Sensor
Thermal desorption process
Tomato seed oil
VOCs

ABSTRACT

Tomato seed oil (TSO) is an edible product characterized by a wide range of molecules, with beneficial effects on human health. Volatile organic compounds (VOC) formed from the degradation of fatty acids, are promising candidates for the characterization of vegetable oils. Hereafter, a sensor based on photoionization detector for palmitic acid is presented. The sensor exploits thermal emission profile analysis from a thin layer of zeolite 5 A. Emissive profiles were acquired through a Photoionization Detector (PID) at 100 °C. Specifically, the combination of use of zeolite with pore size of 5.1 Å and an ultraviolet lamp of 10.9 eV allows selective adsorption and detection of palmitic acid in a solution of pentane and TSO. The PID-zeolite sensor was investigated using oils at different dilution and at different storage conditions (−20 °C, 4 °C and 25 °C). Results evidenced that pentane dilution plays a significant role in palmitic acid adsorption, with a maximum emissive profile at ~885 μmol/L. Low temperature storage (−20 °C) of samples before analysis results in 1.5 times higher emission peak due to the formation of triple chain molecular arrangement of palmitic acid. Calibration evidenced a linear range from 0.45 mmol/L up to 1.8 mmol/L with a sensitivity of 34.65 ppm•mmol$^{-1}$•L and an $R^2$ = 0.92. Real scenario analysis was performed a mixture of TSO with soybean oil (SO) at different storage stability. A significant emissive reduction in palmitic acid was observed in mixed oil, depending on its stability which allows for the evaluation of adulterated samples.

## 1. Introduction

Tomato seed oil (TSO) is a vegetable oil which recently attracted interest due to its nutritional benefits. Even though tomato seeds are generally discarded, their composition is particularly rich in bioactive substances [1–3]. Thus, oil extraction can represent an effective recycling method offering a high nutritional byproduct with significant economic value. TSO is composed by various fatty acids, and many other bioactive compounds, such as vitamin E, carotenoids and polyphenols with high antioxidant and anti-inflammatory properties. These compounds contribute not only to the oxidative stability of oils but also to the organoleptic properties [4]. The latter includes a complex aroma profile and flavor due to the presence of specific volatile organic compounds (VOC). Among them, different fatty acids are well known to have antioxidant properties, as they regulate the synthesis and activity of antioxidant enzymes as well as a positive effect on cholesterol and atherosclerosis [5,6]. Fatty acids are classified into saturated (SFA), monounsaturated (MUFA) and polyunsaturated (PUFA). TSO has been found to be a source of essential PUFA, which cannot be synthesized in the body [7,8]. The main volatile organic compounds of TSO are linoleic, oleic, palmitic, stearic, and linolenic acids. The importance of VOCs as key markers for monitoring biological processes is widely recognized, with significant applications in food quality, human health, and environmental monitoring. However, current technologies for VOC analysis face notable limitations, including complex instrumentation and poor adaptability for real-time or in situ analysis. The standard approach for VOC detection in oil samples consists of high-performance liquid chromatography (HPLC), gas chromatography often combined with mass spectrometry (GC-MS) or with photoionization detector (GC-PID) [9–12]. These challenges highlight the need to focus on the development of sensor systems that can address these drawbacks, enabling more accessible VOC monitoring. The core of the proposed technology is a

* Corresponding author at: Department of Health Sciences, "Magna Græcia" University of Catanzaro, Catanzaro, Italy.
*E-mail address:* pullano@unicz.it (S.A. Pullano).

https://doi.org/10.1016/j.snb.2025.137428
Received 16 December 2024; Received in revised form 11 February 2025; Accepted 11 February 2025
Available online 12 February 2025

sensor that combines the adsorption/desorption capability of a zeolite layer porous to enhance the detection selectivity of a photoionization detector. PID sensor exploits UV radiation with specific energy to ionize molecules with compatible ionization energy (IE). More recently, literature has been focused on developing alternative methods for VOC detection with the aim of having real-time, simple, and, if possible, scalable technologies (e.g., chemosensors, electronic nose, etc.). More recently, literature has been focused on developing alternative methods for VOC detection with the aim of having real-time, simple, and, if possible, scalable technologies (e.g., chemosensors, electronic nose, photoelectrochemical (PEC) sensors, etc.) [13,14]. One of the main drawbacks of PID is the low selectivity of specific molecules, since most of them are very similar in terms of chemical composition and IE. In fact, fatty acids in TSO are characterized by an IE below 10.6 eV [15–17]. Hence, to improve detection selectivity, an alternative technique for VOC analysis was investigated. A thin, porous layer composed of zeolite 5 A coupled with a commercial PID was investigated. Type 5 A zeolite has a well-defined pore size (5.1 Å), a high surface area, and specific mobile metal cations ($Na^{+}$, $Ca^{2+}$) [18]. The layer was realized by spinning and annealing a mixture of zeolite 5 A and soybean oil onto a glass substrate. The structure and the physico/chemical properties of the adsorbent layer were characterized using 3D optical profilometer, scanning electron microscope (SEM) and energy-dispersive spectrometry (EDS), X-ray diffraction (XRD) and Fourier transform infrared (FTIR) spectroscopy. Liquid-phase adsorption, and the subsequent thermally controlled desorption phase was used for the evaluation of the emission profiles of VOCs through a PID. Adsorption dynamics was optimized using specific dilution of TSO in pentane. Moreover, the molecular sieve characteristics of zeolite 5 A, together with the ionization energy of VOCs evidenced the specific adsorption of palmitic acid. Particular attention was given to the variation in palmitic acid concentrations in relation to different storage temperatures, a key factor influencing the overall fatty acid composition of the product. To this end, the crystallization process of certain saturated fatty acids in the TSO was investigated to understand how these physical transitions alter the TSO emission profiles. Specifically, the phase transition of palmitic acid was analyzed to identify the crystalline polymorphs formed at different storage temperatures. Calibration was performed using oil at known concentration of palmitic acid and a real scenario analysis was investigated for the detection of adulterated oil. Blends of TSO and soybean oil at different storage stability were analyzed evidencing the possibility of detecting adulterated samples.

PIDs are not usually suitable for detecting fatty acids, which are larger and less volatile molecules compared to other VOCs. Other detection methods, such as flame ionization detectors (FID) or mass spectrometry, are more commonly used. The proposed approach aims to address the limitations of PIDs by proposing and validating a sensor for the identification of a specific target molecule belonging to the fatty acid class in a real sample. Thus, the development of zeolite-PID sensor capable of providing a rapid and reliable test to assess palmitic acid in TSO can be a reliable alterative technique for analysis and authentication of the samples.

## 2. Experimental section

### 2.1. Zeolite-PID sensor

The VOC detector consists of a sealed metallic chamber equipped with a heating unit and temperature control. The chamber was sized to handle the volume of gas compatible with the capability of the PID detector (500 $cm^3$/min) as shown in Fig. 1 [19].

Specifically, the analysis chamber was realized in aluminum with a volume of 50 $cm^3$ . It includes a 2 mm hole for nitrogen injection, an outlet connector to the PID, and an opening (2 cm x 6 mm) for the zeolite layer insertion. The temperature was set and controlled at 100 °C. The heating is performed by a positive temperature coefficient (PTC) ceramic plate with an aluminum shell. The detector is a commercial PID (MiniRAE 3000, Recom Industriale, Italy) equipped with a 10.6 eV UV lamp, operating at a wavelength of 120 nm with a measurement range up to 15,000 ppm, and a resolution of 0.1 ppm. Linde Type A (LTA) zeolite is a synthetic crystalline material which can be produced in different forms (e.g., 3 A, 4 A and 5 A, etc.), which are distinguished by the presence of potassium, sodium and calcium mobile ions, respectively which are exchanged during the synthesis process The BET surface area of zeolite 5 A typically ranges between 495 $m^2/g$ and 527 $m^2/g$, depending on synthesis conditions and treatments applied. This value

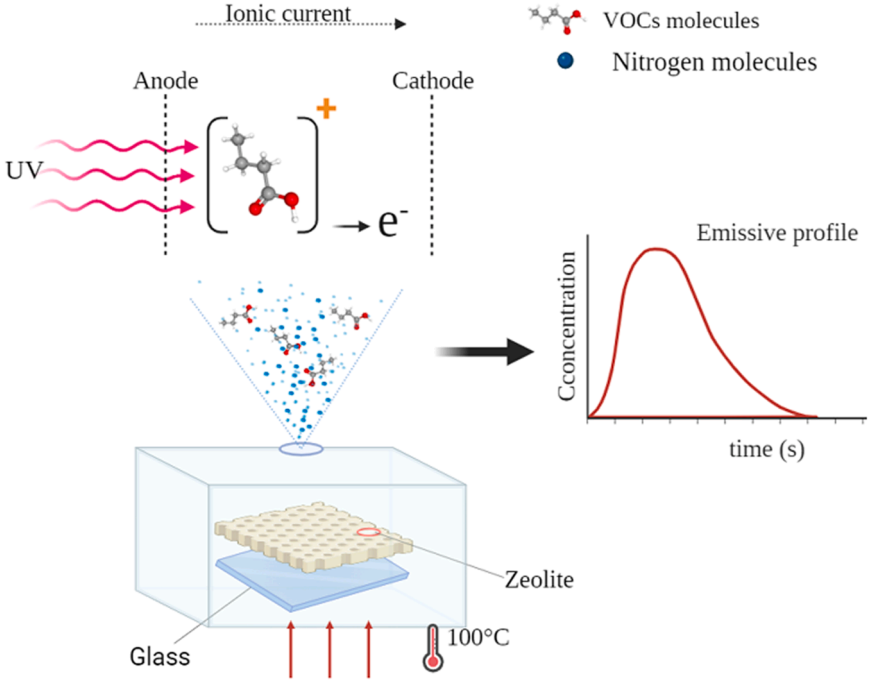


**Fig. 1.** Schematic representation of the PID Zeolite sensor.

confirms its high porosity and efficiency as a molecular sieve. [20,21]. In the framework, Al and Si atoms are connected through O atoms to form a 3D structure of tetrahedra ($AlO_4$ and $SiO_4$) [22–25]. Zeolite 5 A powder (UOP Honeywell, Reggio Calabria, Italy), characterized by a density of 0.548 g/cm$^3$ and pore volume of 0.355 cm$^3$/g was used. Zeolite 5 A is characterized by a pore size of 5.1 Å and $Na^+$ and $Ca^{2+}$ mobile cations. A mixture consisting of 60 % w/w zeolite 5 A and 40 % w/w soybean oil was mixed and stirred for 5 minutes using a homogenizer (IKA, Ultra-Turrax), and sonicated for 5 minutes to reduce particles clustering. A glass coverslip of 18 mm x 18 mm was used as a substrate and a volume of 1 mL spun onto the substrate at 200 rpm for 30 seconds. Subsequently, the sample was annealed at 100 °C for 30 minutes, then the temperature was increased by 50 °C every 30 minutes, reaching a final temperature of 250 °C for 3 hours. Thermal annealing results in the formation of a carbonaceous matrix which keeps the zeolite particles cohesive and attached to the substrate, creating a zeolite-based carbonic matrix. Porous layers were analyzed with a 3D optical profilometer (Vecco, NT 9109). The morphology of the adsorbent layer and the chemical composition were analyzed using scanning electron microscope (Carl Zeiss, EVO HD15) and energy dispersive spectrometry (EDS) at 15 keV (Thermo Scientific, Phenom ProX). FTIR-ATR spectra were acquired using a Thermo Scientific NICOLET 6700, equipped with a Smart iTR™ (i.e. germanium crystal). Each spectrum consists of 50 co-added scans, with a total acquisition time of approximately 100 s and a spectral resolution of 4 cm$^{-1}$, covering the range of 4000–400 cm$^{-1}$. XRD analysis was performed on zeolite powder and annealed mixture using a powder diffractometer APD 2000 equipped with Cu Ka radiation, graphite monochromator, NaI-Tl detector (ItalStructures, Novara, Italy).

### 2.2. TSO sample preparation

A commercial natural cold-pressed unrefined TSO has been obtained from Elemental, Romania and analyzed with HPLC to identify the fatty acid composition. TSO sample contains 44 % of linoleic acid ($C_{18}H_{32}O_2$), 28 % of oleic acid ($C_{18}H_{34}O_2$), 20 % of palmitic acid ($C_{16}H_{32}O_2$), 5 % of stearic acid ($C_{18}H_{36}O_2$), and ~3 % of linolenic acid ($C_{18}H_{30}O_2$). Linoleic acid (C18:2) is an n-6 PUFA, that has two double bonds both having *cis* stereochemistry. Oleic acid (C18:1) is a MUFA with one *cis* double bond at the C9 atom. Palmitic (C16:0) and stearic (C18:0) acids are SFAs without double bonds [26–29]. The analyses were performed using a solution of TSO in pentane ($C_5H_{12}$) at different concentrations. Pentane is an apolar volatile solvent, having a low boiling point (20 °C) if compared to that of TSO (i.e., 130 °C) [26].

### 2.3. Analysis technique

As reported in Fig. 1, the mechanisms that describe the VOC emission rate are regulated by the adsorption and thermal desorption processes. Thermal emission analyses were evaluated using pure TSO sample and diluted TSO sample in pentane down to 0.3 ‰ v/v. Each analysis involves 10 minutes of adsorption phase using 200 µL of diluted TSO sample. Then the sample was rinsed with deionized water and dried under nitrogen flow. Zeolite sample is then placed in the chamber, previously heated at 100 °C, and connected to the PID. Thermal emission was then acquired for 5 minutes to allow a complete desorption from the layer. The thermal emission is expressed in part per million (ppm) of ionized molecules calibrated against the isobutylene.

## 3. Results and discussion

### 3.1. Characterization of zeolite layer

A picture and detailed superficial topology of the zeolite layer is shown in Fig. 2a. It is characterized by an average thickness of 220 µm and a roughness of 1.42 µm (see Fig. 2b). The layer is composed of a carbonaceous matrix in which zeolite 5 A grains are held together by a matrix created by oil decomposition. The hydrophobic nature of soybean oil may enhance the selectivity of zeolite for hydrocarbons (i.e. fatty acids). However, since the soybean oil molecules are mostly larger than the pore sizes of the zeolite, the porous structure is expected to remain unaffected [30]. In Fig. 2c, SEM analysis evidenced that the zeolite layer appears as a homogeneous and compact matrix, composed of individual grains of zeolite with an average size of 2.5 µm. EDS analysis evidenced the presence of C (35.1 %), O (39.9 %), Al (10.60 %), Si (7.80 %), atoms. The latter are due to the zeolite framework and soybean oil decomposition (see Fig. 2d). Mobile cations in the framework are identified in $Ca^{2+}$ constituting the largest percentage (5.20 %) followed by $Na^+$ with a lower concentration (1.4 %). The presence of

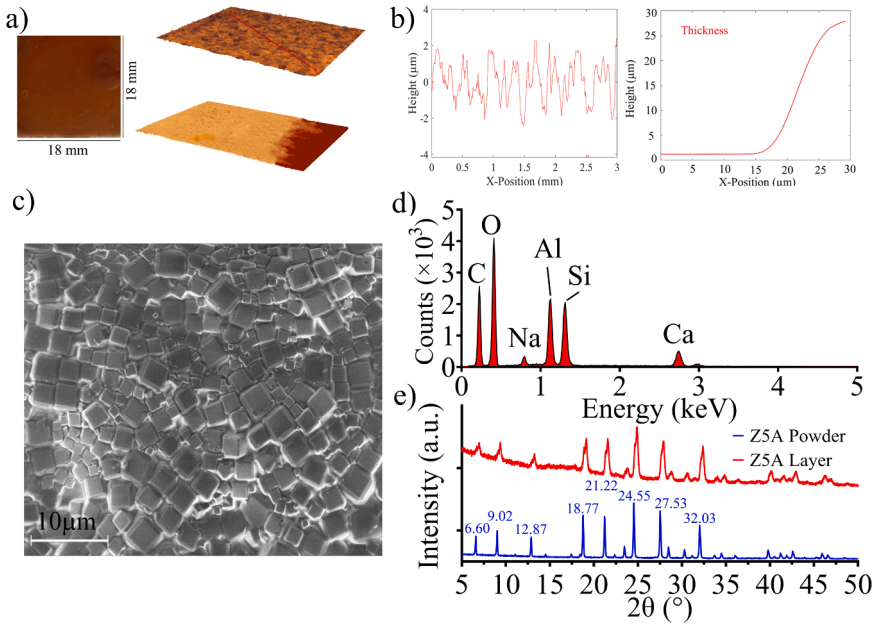


**Fig. 2.** (a) Deposited zeolite layer mixture onto a glass substrate and topographical analysis; (b) roughness and thickness evaluation on a representative sample; (c) SEM image, (d) corresponding EDS spectrum and (e) XRD analysis.

these elements points out that the zeolite layer does not appear to be contaminated by other substances that could affect the thermal emission of specific VOC (see Fig. 2d).

Fig. 2e evidenced the XRD analysis on zeolite 5 A powder and zeolite 5A-soybean oil mixture. Characteristic peaks of zeolite 5 A have been evidenced at 2θ angles of 6.60°, 9.02°, 12.87°, 18.77°, 21.22°, 24.55°, 27.53°, and 32.03°. The results are consistent with literature for dehydrated zeolite Linde Type [31]. The diffractogram of the zeolite 5 A layer also exhibited peaks, with reduced intensity, shifted to higher angles (~ 0.38°), and broadened. Diffraction peaks correspond to zeolite 5 A particles, alongside a broad, diffuse hump that signifies the presence of an amorphous carbonaceous phase, indicating a mixture of ordered and disordered structures. The lower intensity can be associated with higher scattering of the amorphous [32]. Moreover, induced stress within the crystalline structure can also explain the broadened peaks [33,34]. Spectrum of zeolite 5 A layer evidenced an intense absorption around 1000 $cm^{-1}$ due to the Si-O-Si bond and absorption bands in the 500–700 $cm^{-1}$ range, which indicates bending vibrations of the reticular structure. The presence of water within the zeolite is marked by absorption bands associated with OH vibration, with peaks around 3400 $cm^{-1}$ (corresponding to the O-H stretching) and 1640 $cm^{-1}$ (H-O-H bending band) [35]. Interestingly, a peak attributed to the adsorbed O−H vibrations was also observed, but with a distinction, indicating the formation of free water on the catalyst surface [36]. Subsequently, the spectra related to the natural TSO were compared with those found in the literature [37]. The C-H bending vibrations, typical of alkyl chains, are also present in the region between 1460 and 1470 $cm^{-1}$ and around 1370 $cm^{-1}$. The C-H stretching bands of palmitic acid alkyl groups appear in the band from 2850 to 2950 $cm^{-1}$. Additionally, bands attributable to the C═O stretching of saturated fatty acids show a prominent peak around 1740 $cm^{-1}$. These bands provide a distinct fingerprint for palmitic acid [38].

### 3.2. Analysis of thermal emission characteristics and sensing properties

The zeolite layer has been immersed in pure TSO for 10 minutes, rinsed with deionized water and dried under nitrogen flow before FTIR-ATR analysis. The results shown in Fig. 3 evidenced, apart from the characteristic bands of the zeolite. Specifically, the C-H stretching bands of the palmitic acid alkyl chains are observed in the 2850–2950 $cm^{-1}$ range, while the C═O stretching band appears around

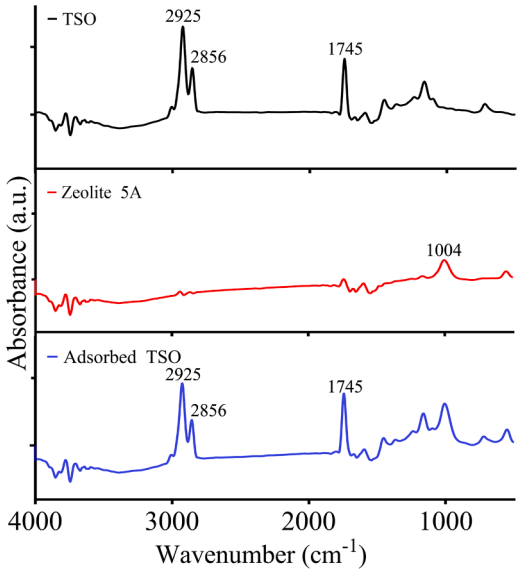


**Fig. 3.** FTIR-ATR spectrum of pure TSO, bare zeolite layer before and after interaction with TSO.

1694 $cm^{-1}$. The C-H bending vibrations, further identifying the alkyl structure, are also observable between 1460 and 1470 $cm^{-1}$ and around 1370 $cm^{-1}$. It is thus plausible that the presence of these bands indicates that the zeolite layer can selectively adsorb palmitic acid from the oil. To further investigate the selective adsorption of palmitic acid, a generic fatty acid was considered which is formed by an acyl chain and a carboxyl group (-COOH). The carboxyl group (-COOH) contains both a hydroxyl group (-OH) and a carbonyl group (C═O). As depicted in Fig. 4a fatty acid can form 2 hydrogen bonds, with atoms in the zeolite framework. The carboxyl group of fatty acid interacts with the zeolite surface (Si-O-Al) through hydrogen bonds, allowing adsorption [38]. Therefore, in general, all fatty acids can be adsorbed onto the zeolite surface. However, considering both zeolite 5 A pore size (5.1 Å) and fatty acids molecular size (see Fig. 4b and Table 1), only palmitic acid is not size excluded and can be adsorbed by the zeolite framework. In fact, while linearized length of all fatty acids is similar, width can be quite different ranging from 5 Å of palmitic acid up to 9.3 Å of linoleic and linolenic acid.

To support this result, Table 1 reports on the physicochemical characteristics of TSO constituents.

Even though all the molecules have IE lower than the PID detector (10.6 eV), potentially all of them could be detected by the PID. The presence of double bonds in fatty acid molecules, such as oleic, linoleic, and linolenic acids, limits their ability to interact with the polar part of zeolite 5 A. This behavior is attributed to the weak hydrogen bonds formed between such molecules and the zeolite layer, which give them greater flexibility and less tendency to adsorb [38]. Consequently, after the adsorption process, when the zeolite layer is rinsed with deionized water and blown under a nitrogen flow, these molecules are easily removed from the surface. In contrast, fatty acid molecules such as palmitic and stearic acid (SFA), free of double bonds, create stronger and more stable interactions with the polar part of the zeolite [39–41]. This results in less structural flexibility and greater adsorption to the layer. Furthermore, since stearic acid in TSO accounts for 5 % for all fatty acids, the observed adsorption can be attributable to palmitic acid. In Fig. 5a the overall prototype of the zeolite-PID sensor is reported. The prototype includes an analysis chamber appropriately drilled with two circular holes: one for PID inlet and one for nitrogen (Fig. 5a, i). Temperature controller, heating plate and a thermocouple are used for maintaining the thermal emission temperature at 100 °C (Fig. 5a ii, iii). All the thermostat system is mounted inside a 3D-printed substrate (Fig. 5a, iv). An opening was used for rapid sample insertion (Fig. 5a, v). All the previous components are coupled with a commercial PID (Fig. 5a, vi). The desorption temperature of 100°C was set to reduce the evaporation phase not affecting the diffusion (which is mostly independent from the temperature). The use of 100°C maximizes the evaporation rate, thus allowing the complete release of VOCs and ensuring accurate detection of their real concentration [19]. Obviously, thermal treatment is also set not to degrade the specific molecule. A reduced volume of analysis to 50 $cm^3$ leads to a higher concentration of VOCs for a shorter time duration compatible with that of PID.

The VOC emission rate during the thermal emission by the zeolite layer can be described as an evaporation and diffusion model:

$$C(t) = E^{-k1t} + D^{-k2t} \quad (1)$$

where C(t) represents the overall emission rate inside the analysis chamber (mg/($m^2$·min)), E (mg/($m^2$·min)) denotes the VOC emission rate regulated by the evaporation process and D (mg/($m^2$·min)) represents the VOC emission rate regulated by the diffusion process. $k_1$ ($s^{-1}$) represents the evaporation coefficient while $k_2$ ($s^{-1}$) is the emission decay constant related to diffusion. Integrating Eq. (1) and assuming zero initial concentration, the model can be rewritten as:

$$C = L\bullet(E\bullet(e^{-k1t} - e^{-nt})/(n-k_1) + D\bullet(e^{-k2t} - e^{-nt})/(n - k_2)) \quad (2)$$

where L is the ratio between the area and volume of the zeolite layer

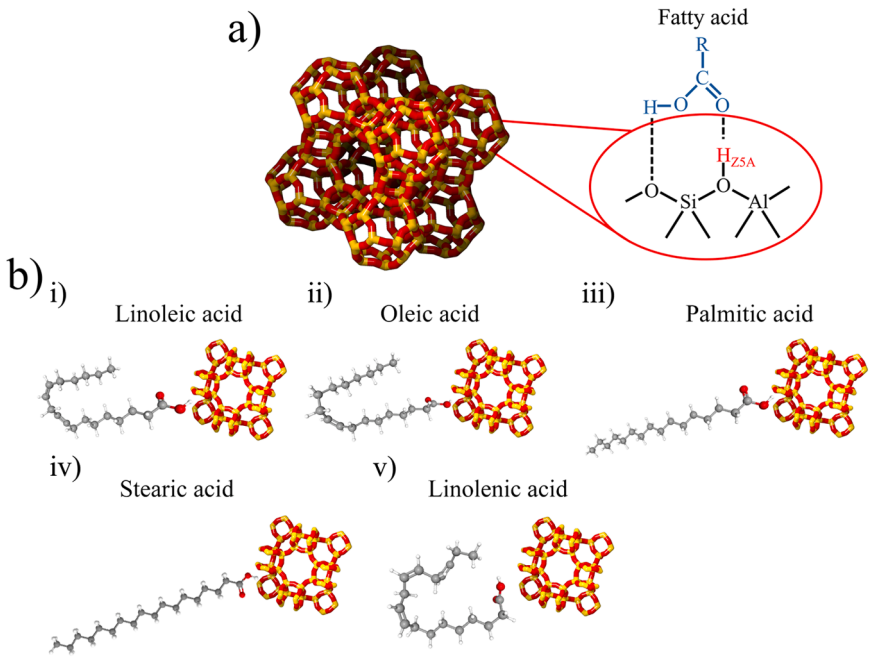


**Fig. 4.** (a) Fatty acid adsorption onto the zeolite 5 A framework and (b) Structure and dimensions of the fatty acids in TSO including (i) linoleic acid, (ii) oleic acid, (iii) palmitic acid, (iv) stearic acid and (v) linolenic acid.

**Table 1**
Physical Characteristics Of Voc.

| Ref. | VOC | Size (Å) | IE (eV) |
|---|---|---|---|
| [29] | *Linoleic acid* | 9.3 × 20 | 8.80 |
| [26,29] | *Oleic acid* | 9.0 × 20 | 8.6 |
| [37] | *Palmitic acid* | 5 × 20 | 9.6 |
| [23] | *Stearic acid* | 5.6 × 21 | 9.75 |
| [25] | *Linolenic acid* | 9.3 × 22 | 8.80 |

($m^2/m^3$), n is the ratio between the nitrogen flows ($m^3/s$) and the chamber volume ($m^3$) [41]. Data acquired from the PID in ppm were converted in $mg/m^3$ to match Eq. (2). Preliminary tests were performed in environmental temperature (25 °C) to evidence any background contributions due to the setup and solvents involved. The emissive profiles of bare zeolite layer, pure pentane, and pure TSO oil adsorbed for 10 minutes onto the zeolite substrate are shown in Fig. 5b. Previous work evidenced as using an adsorption time close to 10 min, the emissive pattern is characterized by a higher amplitude since after longer time low temperature evaporation from the zeolite layer happens [19]. The thermal emission profile is thus characterized by a rapid growth phase, followed by slower decay (e.g., diffusion). During thermal desorption, evaporation occurs quickly as the absorbed molecules are rapidly released from the zeolite layer. As a result, the signal increases very sharply. In contrast, the descending phase, associated with diffusion, is slower, and depends on the gas flow rate analyzed by the PID. The bare zeolite layer did not evidence any background contribution. Conversely, pure pentane results in a background emission with a peak of 0.8 ppm. Pentane can completely evaporate before thermal emission. The ionization energy of pentane (11.8 eV) is higher than the energy of the PID, thus reducing the background contribution. Additionally, pentane allows also a significant reduction in sample viscosity. Pure TSO emissive profile evidenced a trend, which can be described by the evaporation diffusion model characterized by an emissive peak 15 times higher with respect to pentane (see Fig. 5b). In Table 2 are reported the results of fitting model evidencing the evaporation constant $1/k_1$ and emission decay constant $1/k_2$ of pentane and pure TSO emissive profile.

As expected, molecules diffuse in the environment with similar time constant while the evaporation from the substrate occurs at time constant mostly related to the specific characteristics of the molecule. In this case, the higher volatility of pentane can explain the significantly faster evaporation process. To reduce the viscosity of the TSO, diluted samples in pentane were analyzed. Fig. 5c shows the emissive profiles of solutions at different palmitic acid concentrations. Using HPLC data from the TSO sample diluted in pentane (70 % v/v down to 0.3 ‰ v/v) a concentration ranges from 500 mmol/L down to 225 μmol/L was evaluated. Interestingly, the dynamics of profiles from 500 mmol/L down to 7 mmol/L evidenced similar patterns in terms of amplitude and time. Conversely, further dilution down to 225 μmol/L evidenced an increase in amplitude followed by a further sharp decrease as shown in Fig. 5d. The result evidenced that a specific solution of TSO and pentane is desirable to maximize the emissive profile. Such a solution can be seen as a thermodynamic system in which TSO-palmitic acid and palmitic acid-zeolite interactions can take place. Diluted TSO samples in the range from 70 % v/v down to 1 % v/v (500 mmol/L down to 7 mmol/L) have shown that the system is in thermodynamic equilibrium because the concentration of absorbed palmitic acid is constant [40,42–44]. At 0.125 % v/v (885 μmol/L) of diluted TSO in pentane the interactions between polar carboxyl groups of palmitic acid and the surface of zeolite pores prevail enabling the maximum adsorption of palmitic acid since these interactions are energy efficient. Further dilution with pentane causes the occurrence of the desorption process due to a decrease in the binding enthalpy of palmitic acid molecules, which implies that the energy holding the adsorbed molecules to the surface has been reduced enabling the release of molecules. [38,39,43] In addition, interaction between palmitic acid and TSO takes place. A significantly higher concentration was observed at 885 μmol/L, with a maximum peak recorded of ~80 ppm, resulting in 5 times higher than the concentrations detected and reported in Fig. 5d. The repeatability and reproducibility of the sensor were evaluated through intra- and inter-day measurements at 885 μmol/L, resulting in a mean value of 78.64 ppm with a standard deviation of 3.61 ppm. The coefficient of variation (CV) was 4.59 %. The higher emissivity can be attributed to the concentration of adsorbed palmitic acid. In fact, the pentane further reduces the TSO oil density by achieving weak London dispersion forces with the hydrocarboxylic chain of palmitic acid. These interactions are based on temporary

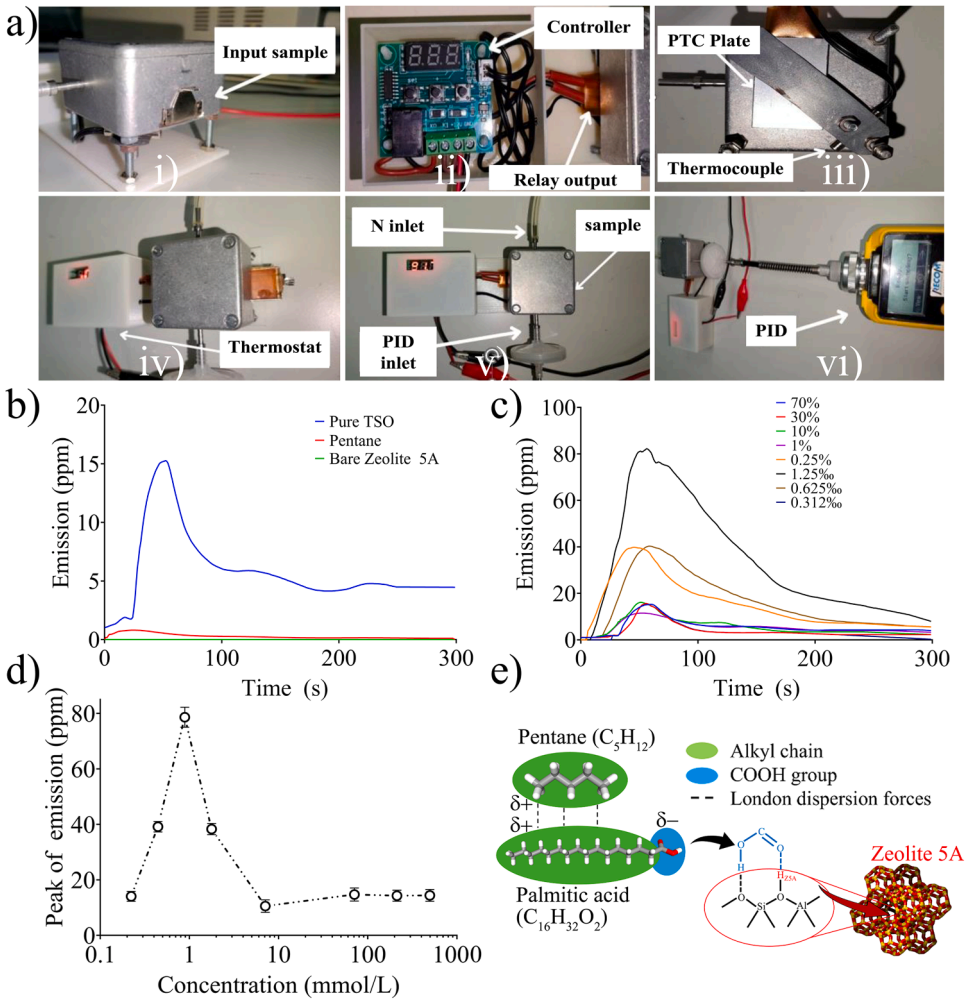


**Fig. 5.** (a) Fabricated PID-Zeolite prototype composed of a thermostat aluminum chamber with included the zeolite 5 A layer and the commercial PID; (b) comparison of thermal emissive profiles of bare zeolite layer and those obtained after adsorption processes of pentane and pure TSO; (c) emissive profiles of palmitic acid molecules with varying TSO sample concentrations; (d) comparison of emission peaks vs TSO/pentane dilution (logarithmic scale) and (e)London interaction in diluted TSO and formation of a hydrogen bonds between the COOH group of palmitic acid and Si-O-Al group of zeolite.

**Table 2**
Non-Linear regression Analysis On pure Pentane and Pure TSO Thermal Emission Profile.

| VOC | $1/k_1$ (s) | $1/k_2$ (s) | E (mg/m$^2$ •s) | D (mg/m$^2$ •s) | L (m$^2$/m$^3$) | n (L/s) |
|---|---|---|---|---|---|---|
| Pentane | 10 | 87.7 | 0.55 | 0.30 | 0.30 | 0.17 |
| Palmitic acid | *35* | *100* | *8.21* | *1.07* | *0.33* | *0.17* |

dipoles resulting from the motion of electrons responsible for the mixing of TSO with pentane [39,44]. At the same time, repulsive interactions may occur between the electron-rich polar carboxyl group (*δ*-) of palmitic acid and the electron cloud (*δ*+) of the nonpolar pentane molecule. Similarly, a strong attractive force appears between the polar carboxyl group (-COOH) of palmitic acid and the polar (Si-O-Al) groups of zeolites, resulting in the formation of hydrogen bonds that connect them [45–49]. This not only enables the anchoring of palmitic acid on the surface but also facilitates its entrapment within the pores of the three-dimensional zeolite framework as shown in Fig. 5e.

Three TSO samples with known palmitic acid concentration in the range 0.45–1.8 mmol/L have been used as reference for PID-zeolite sensor calibration. The corresponding regression was performed as shown Fig. 6a. The results evidenced the PID response was linearly correlated with the palmitic acid concentration. The sensitivity was of 34.65 ppm•mmol$^{-1}$•L with an $R^2 = 0.92$. The proposed technique based on a nanoporous layer of zeolite 5 A in a controlled environment demonstrates the possibility of detecting a specific molecule (i.e., palmitic acid) among chemically similar VOCs in TSO sample. Correct storage of edible oils in general, and thus also the TSO is important to avoid alteration of its organoleptic properties, and therefore of the nutritional grade of the product. The following results have been focused on changes in palmitic acid concentrations related to different TSO storage conditions. Thermal emission profiles at −20 °C, 4 °C and 25 °C are shown in Fig. 6b, evidencing that at lower storage temperature a higher emissivity was observed. Emissive profile at −20°C evidenced a peak of 101.8 ppm, while at 4 °C and 25 °C detected emissive peaks were 89.8 ppm and 69.5 ppm, respectively. The repeatability and reproducibility of the sensor were evaluated at different temperatures. At −20°C, 4°C, and 25°C, the CV was 4.91 %, 2.48 %, and 6.30 %, respectively, with slightly higher variability at 25°C.

As shown in Fig. 6b, oil storage temperature significantly affects the concentration of the detected palmitic acid. The higher emission at –20 °C can be attributed to the crystallization of the SFA fraction of the oil [49]. Because of this phase transition, different crystalline polymorphic structures are formed. Fatty acids can arrange in different types of lateral packing: α polymorph, which is the least stable and β′ and β, which are the more stable form. Looking lengthwise, fatty acid molecules can stack

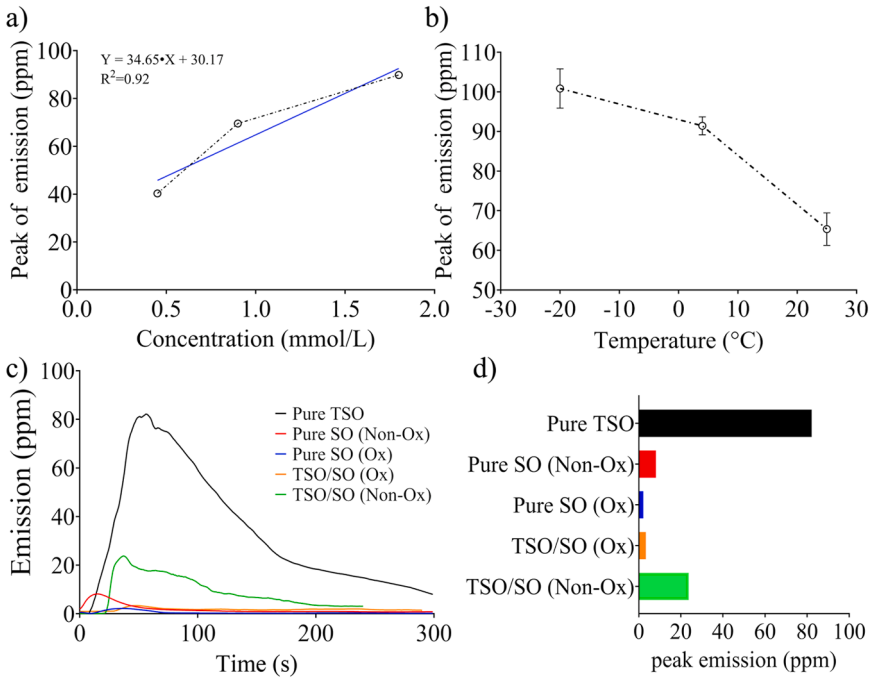


**Fig. 6.** (a) Linear regression of palmitic acid concentration vs peak of emission; (b) emissive peak of TSO stored at different temperatures; (c) comparison among palmitic acid concentration time profiles of pure TSO, soybean oil (SO), and mixed oils and (d) related bar diagram of peak emission.

to form double (2 L), triple (3 L) and quadruple (4 L) chain lengths [48–51]. Differential scanning calorimetry (DSC) analysis by *Barba et al.* reports an exothermic peak at –14.1 °C indicating a phase transition of palmitic (C16:0) and stearic (C18:0) acids. In addition to DSC, synchrotron X-ray diffraction (XRSD) was also used to determine the type of crystalline polymorphs formed [51–53]. It was proved that the exothermic peak at –14.1 °C corresponds to the β′ polymorphs of palmitic and stearic fatty acids [50–52]. Considering the reported polymorph lengths from literature [51,52], and the fact the length of acyl chain -CH2-CH2- is 2.49 Å and that the palmitic acid chain contains 16 C atoms, we evaluated the chain length of 19.92 Å. Thus, the reported length of 59.76 Å can be attributed to the triple chain length of palmitic acid. Since the stearic acid chain contains 18 C atoms, the chain length is 22.4 Å. Thus, the second reported length of 89.64 Å is attributed to the quadrupole chain length of stearic acid. In addition, at –20 °C, a volume contraction of 3.25 % should be considered. However, this cannot explain the higher emission amplitude. Therefore, at –20 °C the probability of finding palmitic acid in the form of tiple chains length molecule significantly increases within respect to 25 °C. The latter results in a higher probability of ionization of 3 molecules at –20°C versus 1 molecule at 25 °C. In addition, one peak was recorded at 2.5 °C indicating partial crystallization of saturated fatty acids in TSO. Using the solid fraction value of the obtained calorimetric melting curve, it is assumed that 17 % w/w of the oil can crystallize during refrigerated storage at 4 °C [50]. Therefore, storage of TSO sample before the analysis can be used as sample concentrator exploiting natural packing of palmitic acid in 3 L chain length molecules.

### 3.3. Application of zeolite-PID sensor

To provide a real scenario analysis, a test was conducted on samples of adulterated oil. Blended oils samples were prepared by mixing TSO oil (50 % v/v) once with highly oxidated commercial soybean oil and once with commercial grade soybean oil. Two samples were prepared using commercial refined soybean oil (SO) at different storage stability: one within the suggested expiration date, well conserved and stored and one long time after the suggested expiration date. Refined vegetable oils are produced using thermal annealing processes for neutralization and deodorization. These processes are used to control acidity and to reduce oxidation, extending the shelf life of the oil. Moreover, they are also performed for odor and volatile components removal [54,55]. Oil oxidation occurs during processing, storage, and heating, leading to the destruction of essential fatty acids and the formation of harmful substances and polymers. While both oils are composed of similar fatty acids profile, highly oxidated soybean oil (stored for several years after the expiration date) is expected to have a very low content of essential fatty acids. As evidenced by the emission profile in Fig. 6c,d the total amount of palmitic acid detected is on average much lower than that shown in pure TSO samples. Conversely, the mixture with SO within the expiration date evidenced a higher emissivity and thus a higher concentration of palmitic acid. For both emission profiles, as it is known, the refining process reduces the quantity of bioactive compounds such as polyphenols and tocopherols that have significant contribution to nutritional value, which results in a lower amount of fatty acids [55,56]. TSO that is rich in linoleic (ω-6 PUFA) and oleic (MUFA) acids can dilute the relative concentration of saturated fatty acids, such as palmitic and stearic acid, in the oil mixture. Pure oil emissive patterns were reported for comparison. When the oil is adulterated, the final fatty acid content results in a weighted average, leading the mixture to have a lower amount of palmitic acid than pure TSO. Therefore, from these results it can be concluded that a rapid and reliable test can be developed not only to determine the quality of the oil, but also to identify adulteration. Such a test would make it possible to quickly verify whether a product has been tampered with, thus ensuring the transparency and reliability of the product to consumers. In accordance with data found in the literature, the crystalline structure of palmitic acid molecule shows that the molecular size is 5 Å. This measurement reflects the overall width of the molecule, thus providing indications of its spatial configuration that affect its physical and chemical behavior. In addition, the ionization energy of palmitic acid molecules results in 9.6 eV. Table 3 reports a non-exhaustive summary of the most recent sensors for palmitic acid detection.

Literature survey on recent palmitic acid sensors evidenced that most of the technologies are based on electrochemical sensors with carbon-

**Table 3**
Representative characteristics of palmitic acid sensors.

| Ref. | Technology | Sensor material | Sensitivity | Linear range | LOD |
|---|---|---|---|---|---|
| [57] | Piezoelectric | PM polyimide | −0.476 $Hz \bullet g^{-1} \bullet dm^3$ | 0.14–0.34 $g\ dm^{-3}$ | - |
| [58] | Electrochemical | rGO/ AuNPs/SPCE | - | 0.192–0.833 mM | $15 \times 10^{-6}$ M |
| [59] | Electrochemical | MIP-MXene/Fc-GO-MWCNT/AuNPs/SPE | $10^{-9}$–$10^{-3}$ M | 0.48–1.61 nM | $0.48 \times 10^{-9}$ M |
| [60] | Electrochemical | rGO/MnNPs/p-Ser | $6.2 \times 10^5$ μA•L•M | 2–10 pM<br>10–100 pM | $8.6 \times 10^{-13}$ M |
| [61] | Colorimetric | polydiacetylenes (PDAs) | | 0–1 M | |
| This work | Photoionization | Zeolite | 34.65 $ppm \bullet mmol^{-1} \bullet L$ | 0.45–1.8 mM | 0.1 ppm |

based sensing materials. To guarantee selectivity, porous membrane is often used as in the case of quartz crystal microbalance-based sensor, in which polymide films were used as selective layers. The linear range of most sensors is useful for the analysis of fatty acids in vegetable or animal oils. However, literature based on palmitic sensor exploiting PID is limited. Most of them are usually combined with other separation techniques, such as GC-PID, GC-FID [62,63]. This study thus demonstrates that while PIDs are not typically used for fatty acid detection, they can be effectively employed when combined with other techniques (i.e. zeolite composite), to enhance selectivity.

## 4. Conclusions

In this work a PID-zeolite sensor was developed and evaluated to detect palmitic acid in TSO oil as an alternative valid method for oil assessment. The sensor is composed by a molecular sieve made of zeolite 5 A inside a metallic chamber maintained at 100°C to allow thermal emission. The latter is detected by molecule ionization generated by UV energy which generates an electric current proportional to the number of ionized molecules per unit volume. The gold standard analysis for the evaluation of fatty acids exploits HPLC or GS according to the European commission and FDA. Recent literature has evidenced that palmitic acid, which belongs to the family of fatty acids, is responsible for many biochemical processes. It is involved in lipid oxidation, which affects shelf life and flavor stability, and plays a role in the texture and structure of fats within foods. In tomato seed oil, a low palmitic acid content is considered favorable since a lower level helps maintain a better lipid profile than oils with a higher saturated fatty acid. The system evidenced a selectivity toward palmitic acid resulting in the possibility of oil analysis without the need of a dedicated laboratory, to detect not only the alterations due to degradation but also fraud and/or manipulation. Analysis also evidenced that the use of −20 °C sample can be used to improve the detection limit of the system acting as a natural concentrator for the oil sample thanks to the 3 L arrangement of palmitic acid molecules The combination of PID and zeolite layer enhances selectivity between chemically similar molecules, making it particularly useful for analyzing complex matrices, such as TSO. This approach also offers the advantage of portability, enabling in-situ real-time monitoring, without the need for complex sample pre-processing. However, limitations include the need for zeolite tailoring, which should be designed for each specific molecule, and the interference from other analytes. Additionally, the ionization energy of the photoionization detector may not always match that of the target VOCs, limiting its effectiveness. In conclusion, the sensor offers a promising solution by balancing performance, cost, and ease of use, with significant potential in industrial and biomedical applications.

## CRediT authorship contribution statement

**G. Oliva**: Conceptualization, Methodology, Validation, Formal analysis, Investigation, Data Curation, Writing - original draft, Writing - review & editing. **L. Manin**: Data curation, Writing - Original Draft, Writing - review & editing. **S. Valic**: Investigation, Resources, Writing - review & editing. **S.K. Islam**: Investigation, Resources, Writing - review & editing. **A.S. Fiorillo**: Conceptualization, Writing - review & editing, Supervision. **S.A. Pullano**: Methodology, Software, Validation, Formal analysis, Resources, Supervision, Project administration

## Declaration of Competing Interest

The authors declare that they have no known competing financial interests or personal relationships that could have appeared to influence the work reported in this paper.

## Acknowledgment

We would like to express our gratitude to Dr. Tatjana Antonić Jelić of Ruđer Bošković Institute for her assistance with the XRD analysis. Open access funding provided by Università degli Studi Magna Graecia di Catanzaro within the CRUI-CARE Agreement.

## Data availability

Data will be made available on request.

## References

[1] K. Szabo, F.V. Dulf, Z. Diaconeasa, D.C. Vodnar, Antimicrobial and antioxidant properties of tomato processing byproducts and their correlation with the biochemical composition, LWT 116 (2019) 108558.
[2] K. Szabo, F.V. Dulf, B.-E. Teleky, P. Eleni, C. Boukouvalas, M. Krokida, N. Kapsalis, A.V. Rusu, C.T. Socol, D.C. Vodnar, Evaluation of the bioactive compounds found in tomato seed oil and tomato peels influenced by industrial heat treatments, Foods 10 (1) (2021) 110.
[3] A. Milani, M. Basirnejad, S. Shahbazi, A. Bolhassani, Carotenoids: biochemistry, pharmacology and treatment, Br. J. Pharmacol. 174 (11) (2017) 1290–1324.
[4] L. Müller, A. Catalano, R. Simone, A. Cittadini, K. Fröhlic, V. Böhm, P. Palozza, Antioxidant capacity of tomato seed oil in solution and its redox properties in cultured macrophages, J. Agric. Food Chem. 61 (2013) 346–354.
[5] O. Aust, W. Stahl, H. Sies, H. Tronnier, U. Heinrich, Supplementation with tomato-based products increases lycopene, phytofluene, and phytoene levels in human serum and protects against UV-light-induced erythema, Int J. Vitam. Nutr. Res 75 (2005) 54–60, 2005.
[6] S. Rizvi, S.T. Raza, F. Ahmed, A. Ahmad, S. Abbas, F. Mahdi, The role of vitamin e in human health and some diseases, Sultan Qaboos Univ. Med J. 14 (2) (2014) e157−e165.
[7] Z.P. Gumus, Z. Ustun Argon, V.U. Celenk, S. Timur, Cold pressed tomato (Lycopersicon esculentum L.) seed oil. Cold Pressed Oils, Academic Press, 2020, pp. 449–458.
[8] C. Carrillo, M. Cavia Mdel, S. Alonso-Torre, Role of oleic acid in immune system; mechanism of action, Nutr. Hosp. 27 (2012) 978–990.
[9] R. Ghosh, S. Luhar, S. Debnath, K.B. Patel, K.V. Baskaran, D.N. Srivastava, P. B. Chatterjee, Measurement of the malignancy marker spermine in human biofluids using smartphone readout and impedance techniques: analytical validation using HPLC, Sens. Actuators B: Chem. 406 (1) (2024) 135390.
[10] J. Lee, H. Min, Y.S. Choe, Y.G. Lee, K. Kim, H.-S. Lee, W. Lee, Highly sensitive and selective detection of benzene, toluene, xylene, and formaldehyde using Au-coated SnO2 nanorod arrays for indoor air quality monitoring, Sens. Actuators B: Chem. 394 (2024) 134359.
[11] N.E. Heshka, Applications of high performance liquid chromatography in the petroleomic analysis of crude oil: a mini-review, Energy Fuels 35 (22) (2022) 18104–18115.
[12] A.W. Boots, A. Smolinska, J.J.B.N. van Berkel, R.R.R. Fijten, E.E. Stobbringh, M.L. L. Boumans, E.J. Moonen, E.F:M. Wouters, J.W. Dallinga, F.J. Van Schooten, Identification of microorganisms based on headspace analysis of volatile organic

compounds by gas chromatography-mass spectrometry, J. Breath. Res 8 (2) (2014) 027106.
[13] Y. Gao, J. Tang, Q. Zhou, Z. Yu, D. Wu, D. Tang, Excited-state intramolecular proton transfer-driven photon-gating for photoelectrochemical sensing of CO-releasing molecule-3, Anal. Chem. 96 (12) (2024) 5014–5021.
[14] Y. Gao, Z. Yu, L. Huang, Y. Zeng, X. Liu, D. Tang, Photoinduced electron transfer modulated photoelectric signal: toward an organic small molecule-based photoelectrochemical platform for formaldehyde detection, Anal. Chem. 95 (23) (2023) 9130–9137.
[15] W. Xu, Y. Cai, S. Gao, S. Hou, Y. Yang, Y. Duan, Q. Fu, F. Chen, Jie Wu, New understanding of miniaturized VOCs monitoring device: PID-type sensors performance evaluations in ambient air, Sens. Actuators B: Chem. 330 (2021) 129285.
[16] S.O. Agbroko, J. Covington, A novel, low-cost, portable PID sensor for the detection of volatile organic compounds, Sens. Actuators B: Chem. 275 (2018) 10–15.
[17] G.C. Rezende, S. Le Calvé, J.J. Brandner, D. Newport, Micro milled microfluidic photoionization detector for volatile organic compounds, Micromachines 10 (4) (2019) 228.
[18] L. García, Y.A. Poveda, M. Khadivi, G. Rodriguez, O. Görke, H.R. Godini, G. Wozny, A. Orjuela, Synthesis and granulation of a 5A zeolite-based molecular sieve and adsorption equilibrium of the oxidative coupling of methane gases, J. Chem. Eng. Data 62 (4) (2017) 1550–1557.
[19] G. Oliva, A.S. Fiorillo, S.K. Islam, S.A. Pullano, Detection of propionic acids trapped in thin zeolite layer using thermal desorption analysis, Sensors 23 (2023) 7352.
[20] T. Li, S. Wang, J. Gao, R. Wang, G. Gao, G. Ren, S. Na, M. Hong, S. Yang, Spherical binderless 4A/5A zeolite assemblies: synthesis, characterization, and adsorbent applications, Molecules 29 (7) (2024) 1432.
[21] L. Chen, J.-Y. Qian, C. Yang, P.-P. Xu, D.-D. Zhu, J. Zhong, M.-Y. He, Q. Chen, Z.-H. Zhang, Direct synthesis of 5A zeolite from palygorskite: the influence of crystallization directing agent on the separation performance for hexane isomers, Clays Clay Miner. 68 (2020) 1–1438.
[22] G. Oliva, M.G. Bianco, A.S. Fiorillo, S.A. Pullano, Anti-reflective zeolite coating for implantable bioelectronic devices, Bioengineering 2022 9 (8) (2022) 404.
[23] G. Oliva, A.S. Fiorillo, T. Antonić Jelić, S. Valić, S.A. Pullano, Thermal desorption from zeolite layer for VOC detection, Solid-State Electron. 210 (2023) 108809.
[24] G. Oliva, A.S. Fiorillo, Detection of Volatile Organic Compounds Adsorbed Onto Zeolite Layers. IEEE International Symposium on Medical Measurements and Applications (MeMeA), Messina, Italy, 2022, pp. 1–5.
[25] M.A. Dreyfus, M.V. Johnston, Rapid sampling of individual organic aerosol species in ambient air with the photoionization aerosol mass spectrometer, Aerosol Sci. Technol. 42 (1) (2010) 18–27.
[26] K. Fumitoshi, Y. Kazuhiro, K. Kenj, K. Takashi, K. Masamichi, Structure and crystallization behavior of the β phase of oleic acid, J. Phys. Chem. B 101 (1997) 1803–1809.
[27] E.Yon Sydow, On the structure of the crystal form B of stearic acid, Acta Cryst. 8 (1955) 557.
[28] A.R. Verma, Interferometric and X-ray investigation of the growth of long-chain fatty acid crystals I. Polymorphism and polytypism in palmitic acid crystals, Proc. R. Soc. Lond. 1778 (1955) 1172. A22834–50.
[29] E.R. Mysak, K.R. Wilson, M. Jimenez-Cruz, M. Ahmed, T. Baer, Synchrotron radiation based aerosol time-of-flight mass spectrometry for organic constituents, Anal. Chem. 77 (2005) 5953–5960.
[30] S. Lu, Y. Ma, S. Shen, C. Zhu, The effect of dydrophobic modification of zelites on CO2 absorption in different solvents, Braz. J. Chem. Eng. 27 (2) (2010) 327–338.
[31] M.J. Treacy, J.B. Higgins. Collection of Simulated XRD Powder Patterns for Zeolites, 4th edn, Elsevier, Amsterdam, 2001, p. 379.
[32] M. Hua, Y. Xu, Y. Duan, C. Zhu, J. Liu, M. Song, Flue gas HgO removal by FeCl3 -impregnated LTA and MFI zeolites: influences of topology and cation sites, EnergyFuels 34 (8) (2020) 9903–9913.
[33] K.H. Tan, H.Y. Cham, H. Awala, T.C. Ling, R.R. Mukti, K.L. Wung, S. Mintova, E. P. Ng, Effect of extra-framework cations of LTL nanozeolites to inhibit oil oxidation, Nanoscale Res Lett. 10 (1) (2015) 253.
[34] X.Hoan Vu, U. Armbruster, Engineering of zeolite crystals for catalytic cracking of triglycerides to renewable hydrocarbon fuels and chemicals: a review, Biomass-.-. Convers. Biorefinery 13 (2021) 3521–3541.
[35] I. Solaberrieta, A.C. Mellinas, J. Espagnol, M. Hamzaoui, A. Jiménez, M. C. Garrigós, Valorization of tomato seed by-products as a source of fatty acids and bioactive compounds by using advanced extraction techniques, Foods 11 (2022) 2408.
[36] Z. Yu, Z. Xu, R. Zeng, M. Xu, M. Zou, D. Huang, Z. Weng, D. Tang, Tailored metal-organic framework-based nanozymes for enhanced enzyme-like catalysis, Angew. Chem. Int Ed. Engl. 18 (2024) e202420200.
[37] Y. Iwai, M. Uno, H. Nagano, Y. Arai, Measurement of solubilities of palmitic acid in supercritical carbon dioxide and entrainer effect of water by FTIR spectroscopy, J. Supercrit. Fluids 28 (2004) 193–200.
[38] D. Kerstens, S. Van Praet, L. Verhoeven, P. Struelens, B.F. Sels, Branched fatty acids: the potential of zeolite catalysis, ACS Sustain. Chem. Eng. 10 (15) (2022) 4807–4817.
[39] T. Liang, B. Wang, Z. Fan, Q. Liu, A facile fabrication of superhydrophobic and superoleophilic adsorption material 5A zeolite for oil–water separation with potential use in floating oil, Open Phys. 19 (2021) 486–493.
[40] A.A. Vasconcelos, T. Len, Ad.N. de Oliveira, A.A.Fd Costa, A.Rd.S. Souza, C.E. Fd Costa, R. Luque, G.Nd Rocha Filho, R.C.R. Noronha, L.A.Sd Nascimento, Zeolites: a theoretical and practical approach with uses in (bio)chemical processes, Appl. Sci. 13 (3) (2023) 1897.
[41] G. De Gennaro, A. Demarinis Loiotile, R. Fracchiolla, J. Palmisani, M.R. Saracino, M. Tutino, Temporal variation of VOC emission from solvent and water based wood stains, Atmos. Environ. 115 (2015) 53–61.
[42] A.F. Mayta-Armas, Y. Canchanya-Huaman, J. Pomalaya-Velasco, Y. Bendezú-Roca, N.-R. Checca-Huaman, J.A. Ramos-Guivar, Enhanced removal of As(V) and Pb(II) from drinking and irrigating water effluents using hydrothermally synthesized zeolite 5A, Water 15 (10) (2023) 1892.
[43] H.N. Tran, E.C. Lima, R.S. Juang, J.C. Bollinger, H.P. Chao, Thermodynamic parameters of liquid–phase adsorption process calculated from different equilibrium constants related to adsorption isotherms: a comparison study, J. Environ. Chem. Eng. 9 (6) (2021) 106674.
[44] B.A. Grigoryev, Yu.L. Rastorguyev, D.S. Kurumov, A.A. Gerasimov, V.E. Kharin, S. A. Plotnikov, Thermodynamic properties of n-pentane, Int J. Thermophys. 11 (1990) 487–502.
[45] B.H. Sage, W.N. Lacey, Phase equilibria in hydrocarbon systems. thermodynamic properties of n-pentane, Ind. Eng. Chem. 34 (6) (1942) 730–737.
[46] J. Vera, Molecular thermodynamics of fluid-phase equilibria by J.M. Prausnitz, R. N. Lichtenthaler, E. Comes de Azevedo, Third Edition, 1999; Prentice Hall PTR, Upper-Saddle River, New Jersey, CAN. J. CHEM. ENG. - CAN J. CHEM ENG 78 (2000) 429–430.
[47] S. Neogi, R. Ghosh, Influence of dipole moment on the VOC sensing properties of BiFeO3 microspheres: addressing the selectivity towards acetone, Sens. Actuators B: Chem. 415 (2024) 135980.
[48] J.M.C. Marques, F.V. Prudente, F. Pirani, Intermolecular forces: from atoms and molecules to nanostructures, Molecules 27 (2022) 3072.
[49] X. Li, Y. Zhao, S. Wang, Y. Zhu, G. Yang, DFT-D2 study of the adsorption of bio-Oi model compounds in HZSM-5: C1–C4 carboxylic acids, Catal. Lett. (2016) 146.
[50] L. Barba, G. Arrighetti, S. Calligaris, Crystallization and melting properties of extra virgin olive oil studied by synchrotron XRD and DSC, Eur. J. Lipid Sci. Technol. 115 (3) (2013) 322–329.
[51] K. Sato, Solidification and phase transformation behaviour of fats – a review, Fett-Lipid (12) (1999) 467–474.
[52] A.G. Marangoni, N. Acevedo, F. Maleky, F. Peyronel, G. Mazzanti, B. Quinn, D. Pink, Structure and functionality of edible fats, Soft Matter 8 (2012) 1275–1300.
[53] G. Keller, F. Lavigne, L. Forte, K. Andrieux, M. Dahim, C.M. Ollivon, C. Bourgaux, P. Lesieur, DSC and X-ray diffraction coupling, Specif. Appl., J. Therm. Anal. 51 (1998) 783–791.
[54] J. Costa, I. Mafra, J.S. Amaral, M.B.P.P. Oliveira, Monitoring genetically modified soybean along the industrial soybean oil extraction and refining processes by polymerase chain reaction techniques, Food Res. Int. 43 (1) (2010) 301–306.
[55] F. Fine, C. Brochet, M. Gaud, P. Carre, N. Simon, F. Ramli, F. Joffre, Micronutrients in vegetable oils: the impact of crushing and refining processes on vitamins and antioxidants in sunflower, rapeseed and soybean oils, Eur. J. Lipid Sci. Technol. 118 (5) (2015) 680–697.
[56] R.D. O'Brien, in: L.A. Johnson, P.J. White, R. Galloway, Soybeans (Eds.), 12 - Soybean Oil Purification, AOCS Press, 2008, pp. 377–408.
[57] O.V. Duvanova, I.A. Krivonosova, A.N. Zyablov, A.V. Falaleev, V.F. Selemenev, S. A. Sokolova, Use of piezoelectric sensors for the determination of oleic and palmitic acids in vegetable oils, Inorg. Mater. 54 (2018) 1387–1391.
[58] C.B. Ching, J. Abdullah, N.A. Yusof, Reduced graphene oxide/gold nanoparticles modified screen-printed electrode for the determination of palmitic acid, J. Sens. 2021 (2021) 6684770.
[59] H. Zhang, Development of surface molecular-imprinted electrochemical sensor for palmitic acid with machine learning assistance, Talanta 275 (2024) 126124.
[60] M.F. Falone, B.G. Olsena, E. Buffon, N. Ramos Stradiotto, Electrochemical sensing of palmitic acid in guava oil using a surface modified with reduced graphene oxide-decorated manganese nanoparticles and electropolymerized poly(L-serine) film, Journal of Food Composition and Analysis, 135(2024), 106550..
[61] N. Kaewnukulkit, N. Traiphol, R. Traiphol, Colorimetric sensing of fatty acids in organic solvents using polydiacetylene-based nanocomposites, Heliyon 10 (2024) e38708.
[62] P. Xiaobing, L. Wenke, W. Shuaiqi, W. Zhentao, S. Songhua, L. Yan, C. Dongzhi, L. Haiyan, Application of homemade portable gas chromatography coupled to photoionization detector for the detection of volatile organic compounds in an industrial park, J. Chromatogr. A 1704 (2023) 464089.
[63] S. Muhammad Alinafiah, A. Azlan, A. Ismail, N.-K. Mahmud Ab Rashid, Method development and validation for omega-3 fatty acids (DHA and EPA) in fish using gas chromatography with flame ionization detection (GC-FID), Molecules 26 (2021) 6592.

**Giuseppe Oliva** is a Ph.D. student in Life Sciences and Technologies at Magna Graecia University of Catanzaro. He spent a research period as a visiting student at the College of Engineering, University of Missouri, USA. He received his bachelor's degree in computer and biomedical engineering and his master's degree in biomedical engineering from Magna Graecia University of Catanzaro. His research focuses on the development of sensors for the detection of volatile organic compounds (VOCs) using nanoporous materials, such as zeolite, combined with photoionization systems. His research activities are mainly aimed at the development of VOC monitoring systems for environmental and human health safety applications.

**Laura Manin** received her bachelor's and master's degree in environmental and public health from the Faculty of Medicine - University of Rijeka, Croatia. She is a visiting trainee at the Department of Health Sciences - University Magna Græcia of Catanzaro, Italy, under the Erasmus + program. She received the Rector's Award for the Student of the Generation in 2024. She was participating in the CEEPUS International Summer School on "Food

Safety and Healthy Living" at the Biotechnical Faculty in Ljubljana in 2023. She is Member of the Organizing Committee and Editor in Chief of Student Health Protection Congress – Sanitas. Her research interests include the antioxidant properties of industrial by-products using Electron Spin Resonance (ESR), mechanisms of action of plant and animal toxins, nanoporous materials for application in medicine.

**Srećko Valić** is Full professor of Physical Chemistry at the Faculty of Medicine - University of Rijeka, Croatia. He is also a Senior Scientist at the Ruđer Bošković Institute, Zagreb, Croatia. He graduated in physics and chemistry at the University of Rijeka, Croatia in 1986, and obtained PhD degree in chemistry in 1993 at the University of Zagreb, Croatia. He spent three years as a postdoctoral fellow at Laboratoire de Physique des Solides, Université Paris-XI, France and one year at the Institut für Makromolekulare Chemie in Freiburg, Germany as a fellow of the Alexander von Humboldt Foundation. His research interests are molecular dynamics and structure of polymers and composite materials. In his research work, he uses spectroscopic techniques (ESR NMR and FTIR) and thermal analysis methods (DSC and TGA).

**Syed Kamrul Islam** received the B.Sc. degree in electrical and electronic engineering from Bangladesh University of Engineering and Technology (BUET), Dhaka, Bangladesh, and the M.S. and Ph.D. degrees in electrical and systems engineering from the University of Connecticut, Storrs, CT, USA. He is currently a Professor and the Chair of the Department of Electrical Engineering and Computer Science (EECS), University of Missouri, Columbia, MO, USA. Before July 2018, he was a James W. McConnell Professor and the Associate Head of the Department of EECS, The University of Tennessee, Knoxville, TN, USA. His research interests include semiconductor devices, analog and mixed-signal circuit design, bio-microelectronics, and circuits and systems for machine learning. In recognition of his teaching, research, and related efforts, he received the John W. Fisher Professorship, the Moses E. and Mayme Brooks Distinguished Professor Award, the Gonzalez Family Award for Excellence in Teaching, the ECE Faculty of the Year Award, and the Alexander Prize.

**Antonino S. Fiorillo** is a Full Professor of Electronic Engineering and Sensors and Electronic Systems at the University Magna Græcia of Catanzaro, Italy. He was visiting scientist from 1987to 1997, and then visiting professor from 1997 to 2002 at the "Center of Sensor Technologies" of the University of Pennsylvania, PA. From 1984–1991 he was a research scientist at the "Centro E. Piaggio" School of Engineering, at the University of Pisa. He had been an assistant professor at the University of Salerno and the University of Sannio, from 1991 to 2003. Dr. Fiorillo received his degree in Electronic Engineering and his Ph.D. in Electronic Devices and Technologies, both at the University of Pisa, Italy. He is a Life Senior Member of the IEEE. He is named in the World's top 2 % Scientists of the Stanford ranking. He is the author of over 200 journal and conference papers and 11 patents. He is the General Conference Chair of the International Workshop of Biomedical Applications Technologies and Sensors (BATS) and qBATS. He was involved in the development of proximity and tactile sensors for robots, promoting the development of the first wide-band cochlear-like transducer. His primary research interests are in the area of discrete and silicon integrated sensors based on ferroelectric and conducting polymers, as well as nanoporous materials, for application in the fields of robotics and medicine. In this context, bio-inspired systems are investigated with emphasis on the interfacing of electronic sensors and biological systems for direct electrical brain stimulation.

**Salvatore A. Pullano** is an Associate Professor of Electronics at the University Magna Græcia of Catanzaro, Italy and Adjunct Assistant Professor at the University of Missouri - Columbia, USA. He was visiting scholar at the Department of Electrical Engineering and Computer Science, University of Tennessee, Knoxville USA. He received his Bachelor's and Master's degree in Electronic Engineering from the University of Calabria, Italy, and his Ph.D. in Biomedical Engineering and Computer Science from the University Magna Græcia of Catanzaro, Italy. He is the author of over 120 journal and conference papers and patents. His research interests include the design of ferroelectric sensors, iono-electronic interfaces and nanoporous materials for biomedical applications.